Research Article

Bi-Template Assisted Sol-Gel Synthesis of Photocatalytically-Active Mesoporous Anatase TiO_2 Nanoparticles

Abubakar Hamisu and Umar Ibrahim Gaya*
Department of Pure and Industrial Chemistry, Bayero University Kano, Kano State, Nigeria

Abdul Halim Abdullah
Department of Chemistry/Institute of Advanced Technology, Universiti Putra Malaysia, Selangor D.E., Malaysia

* Corresponding author. E-mail: uigaya.chm@buk.edu.ng DOI: 10.14416/j.asep.2021.04.003
Received: 8 February 2021; Revised: 12 March 2021; Accepted: 25 March 2021; Published online: 23 April 2021

Abstract
Sol-gel mesoporous titanium dioxide powders have been synthesized from chitosan and/or hexadecyltrimethylammonium bromide (HDTMA) and characterized using x-ray diffraction (XRD), scanning electron microscopy (SEM), transmission electron microscopy (TEM), ultraviolet-visible (UV-vis) spectroscopy, thermogravimetric analysis (TGA), differential thermal analysis (DTA) and N_2 adsorption-desorption measurements. The photocatalytic performance of the synthesized meso-TiO_2 powders was optimized based on the central composite design (CCD) of methyl orange (MO) degradation under UV light irradiation. The maximum MO degradation was 62.3% over a period of 60 min. Oxides produced using the binary chitosan and HDTMA template (C,H-TiO_2) exhibited the relatively higher surface area (99.5 m^2/g), smaller crystal size (12.78 nm), narrower band-gap energy (2.92 eV) and higher photocatalytic rate constant (0.0112 min^{-1}) than as those from chitosan (C/TiO_2) or HDTMA (H/TiO_2) as the template.

Keywords: Mesoporous, TiO_2, anatase, Bi-Template, photocatalysis, Sol-Gel

1 Introduction

Azo dyes, such as methyl orange (MO), are well known for their toxicity [1], [2], recalcitrance, and insusceptibility to conventional biological or physical treatment methods [3], [4]. Typically, the levels of these dyes (~500 mg/L) in textile effluents are barely tolerable [5]. Metal oxide semiconductors with high activity such as TiO_2, have the potential to cause the complete destruction of such non-biodegradable dye pollutants [6]–[8]. However, the efficiency of TiO_2 photocatalysis is reduced by electron/hole transfer limitations and charge carriers recombination [9], particle aggregation (which hinders light absorption) [10] and high band gap energy [11]. To tackle these challenges, various attempts were made to control TiO_2 properties such as structure, morphology and porosity. Currently, the control strategies include metal/non-mental doping, construction of metal or semiconductor heterojunctions, chemical modification of surface, and fabrication of nanostructures [12]–[14].

Templating technique has been an idealized to predetermine and control the internal and external titanium dioxide structures such as morphology, dimension and shape, pore structure, surface area, crystallinity and size distributions [15]–[17]. Various kinds of templates such as surfactant, homopolymer, block copolymer and small organic molecules have been successfully used in the preparation of mesoporous TiO_2 structure [18]–[22]. These titanium oxides exhibit

Please cite this article as: A. Hamisu, U. I. Gaya, and A. H. Abdullah, "Bi-template assisted sol-gel synthesis of photocatalytically-active mesoporous anatase TiO_2 nanoparticles," *Applied Science and Engineering Progress*, vol. 14, no. 3, pp. 313–327, Jul.–Sep. 2021, doi: 10.14416/j.asep.2021.04.003.

high surface area, large pore volume, tunable pore size, pore shape [23] and increased active site density [24], for application in adsorption, catalysis, separation, sensing and biotechnology [23]. The improvement of TiO_2 mesoporosity enhances interaction with chemical species, the transfer of light-excited carrier to the particle surface, and diffusion at the surface [25], [26], and promotes the physical and chemical properties of this material for successful application [27].

Chitosan (or (1,4)-2-amino-2-deoxy-β-D-glucan), a hydrophilic derivative of chitin biopolymer, has been singly utilized as a template for the synthesis of high surface area, hybrid mesoporous aluminium and silicon oxides spheres [28], sol-gel based mesoporous TiO_2–curcumin nanoparticles [29], and a high surface area porous silica [30]. Similarly, hexadecyltrimethylammonium bromide (HDTMA; $[(C_{16}H_{33})N(CH_3)_3]Br$) has been used as template for synthesis of mesoporous TiO_2/ZnO [31], mesoporous TiO_2 nanotube [32] and mesoporous silica [33]. In this work, chitosan and HDTMA are employed for the first time as a bi-template to synthesize new mesoporous TiO_2 nanoparticles, whose photocatalytic activity was assessed using aqueous methyl orange (MO) under UV light irradiation. The choice of these templates was dictated by their hydrophilicity, low molecular weight and decomposition temperature, which are desirable for obtaining stable titania mesostructure [21], [34].

2 Experimental

2.1 *Chemicals*

Titanium (IV) butoxide (99%) was purchased from ACROS Organics. A low molecular weight chitosan (ID 448869 ; 75 to 85 % deacetylated; MW = 50,000 to 190,000 g/mol) was purchased from Aldrich. Hexadecyltrimethylammonium bromide (HDTMA) was purchased from Fluka. Glacial acetic acid, methyl orange (85%), H_2SO_4 (95–98%) and NaOH (98%), were supplied by R & M Chemicals.

2.2 *Catalyst synthesis*

The mesoporous TiO_2 nanoparticles were synthesized by a sol-gel method. Solution A was prepared by mixing equal volumes (12 mL) of chitosan solution (3 g dissolved in 50 mL of 10% acetic acid) and HDMA solution (3 g dissolved in 50 mL of deionized water) and stirring for 30 min. Solution B was prepared by adding 10 mL of titanium (IV) butoxide to 20 mL glacial acetic acid, followed by stirring vigorously for 30 min. Subsequently, the mixture of solution A was slowly added to solution B, with vigorous stirring, continued for 2 h. The resulting mixture was kept at room temperature in a dark for 24 h, followed by gelation at 75°C for 12 h and drying at 120°C for 5 h. The dry gel was calcined in air at 500°C for 4 h. Because of the use of bi-template (chitosan and HDMA) this material was labeled C,H/TiO_2. Other materials labelled C/TiO_2, H/TiO_2 or W/TiO_2 were prepared using only chitosan, HDMA or devoid of template, respectively.

2.3 *Catalyst characterisation*

The surface area and pore volume of the catalysts (previously degassed at 200°C for 2 h) were determined by N_2 adsorption-desorption experiment at 77.322 K using Micromeritics 3Flex 1.02 instrument. The X-ray diffraction (XRD) patterns of these materials were recorded on Shimadzu XRD-6000 X-ray diffractometer operated in the 2θ range of 20–80°, using Cu Kα radiation (λ = 0.15406 nm). Average crystallite size was determined using Debye-Scherrer equation [Equation (1)].

$$\text{Size} = \frac{K\lambda}{\beta \text{Cos}\theta} \quad (1)$$

Where K is a constant 0.93, λ = 0.15406 nm is the wavelength of Cu Kα X-ray, β is the full width at half-maximum (FWHM) of the diffraction peak, and θ the diffraction angle.

The morphologies of the photocatalysts were examined using NOVA NANOSEM 230 field emission scanning electron microscope (FE-SEM) equipped with energy dispersive X-ray facility for elemental analysis, and a JEM-2100F Field Emission TEM equipped with ImageJ software (Java 1.6.0). The degradation efficiencies of MO were calculated based on ultraviolet-visible (UV-vis) spectrometry using a Lambda 35 Perkin Elmer facility. The estimation of band-gap energy was performed on Shimadzu UV-3600 UV-Vis-NIR spectrometer, in the range of 220–800 nm, using $BaSO_4$ as the reference. Thermo-gravimetric analysis (TGA) and differential thermal analysis (DTA) were conducted on TGA/DSC 1 (STAR^e System, METTLER TOLEDO) by heating

10 mg initial mass of the photocatalyst from room temperature to 800°C at the rate of 10°C/min, under air atmosphere.

2.4 *Photocatalytic test*

The photocatalytic performance of the synthesized TiO_2 was followed by measuring the percentage degradation of methyl orange (MO) under UV light irradiation. Experiments were conducted in a known photoreactor [35], fitted now with a China model E14 GMY 3 W UV lamp having UV intensity of 450 μw/cm^2 and wavelength of 253 nm, respectively. Initially, a solution containing a desired amount of MO and catalyst was added to the photoreactor, and the pH of the solution was adjusted by addition of either NaOH or H_2SO_4. The concentration of dissolved oxygen was maintained by continuously bubbling oxygen into the mixture. Samples were taken at every 20 min interval, filtered using 0.45 μm cellulose nitrate membrane to remove the catalyst and analyzed using a Perkin-Elmer, Lambda 35 UV-Vis spectrometer at wavelength of 465.4 nm. Percentage degradation (%D) of the initial MO concentration was calculated using Equation (2).

$$\%D = \frac{[MO]_o - [MO]_t}{[MO]_0} \times 100 \quad (2)$$

Where $[MO]_o$ is the initial methyl orange concentration, $[MO]_t$ is the concentration of methylene blue at irradiation time, t. Blank tests were carried out under irradiation devoid of TiO_2 and in the dark with TiO_2.

2.5 *Design of experiment*

Having relatively the best photocatalytic properties, the performance of meso-TiO_2 derived from two templates (C,H/TiO_2) was optimized based on MO degradation, employing a three-variable, rotatable, central composite design (CCD) and analyzed using Design-Expert version 6.0.6. The independent parameters selected were TiO_2 loading, initial concentration of MO and pH organized combination of levels at center points, factorial points and axial points (as shown in Figure 1). The Figure 1 shows the factorial points at the vertices of a cube box with coordinates (which are combinations of –1 and +1) and the center points at 0,0,0. The axial points manifest

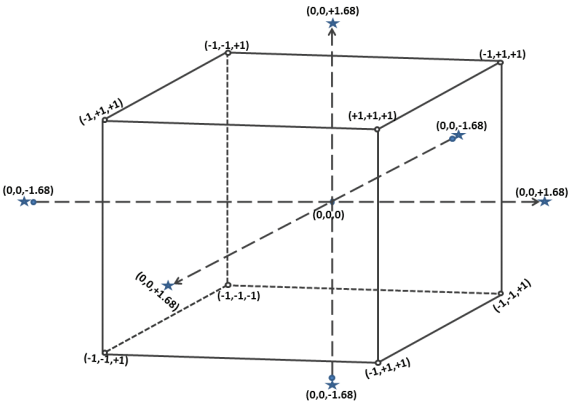

Figure 1: Schematic representation of the central composite design used in this study.

at a distance ± α = 1.68 from the central coordinates.

Table 1 shows the actual levels of pH (2.5, 4, 5.5, 7, 8.5), C,H/TiO_2 (0.25, 0.5, 1. 1.5, 2 g/L) and MO (15, 20, 25, 30, 35 mg/L), as represented by the codes (–1.68, –1, 0, +1, +1.68) in Figure 1. Actually, in accordance with Equation (3) [36], twenty experiments were performed each lasting for 60 min, with eight of the experiments at the factorial points, six experiments at the axial points, and six replications at the center point.

$$N = 2^n + 2n + n_c = 2^3 + 2(3) + 6 = 20 \quad (3)$$

Where N is the total number of experiments required, n is the number of factors and n_c is replications at center. The experimental design matrix were processed based on a suitable model to obtain statistically acceptable, predicted degradation efficiencies and a model equation. Maximum efficiencies were generated by numerical optimization. The optimized values were validated by averaging out repeated experiments. Subsequently, to determine kinetic parameters, experiments were performed for 120 min and kinetic profiles were plotted according to pseudo-first-order integrated rate equations.

Table 1: Factors and their levels for two factor-three level central composite design

Factor	Codes and Levels				
	–1.68	**–1**	**0**	**+1**	**+1.68**
C,H/TiO_2 (g/L)	0.25	0.5	1	1.5	2
[MO] (mg/L)	15	20	25	30	35
pH	2.5	4	5.5	7	8.5

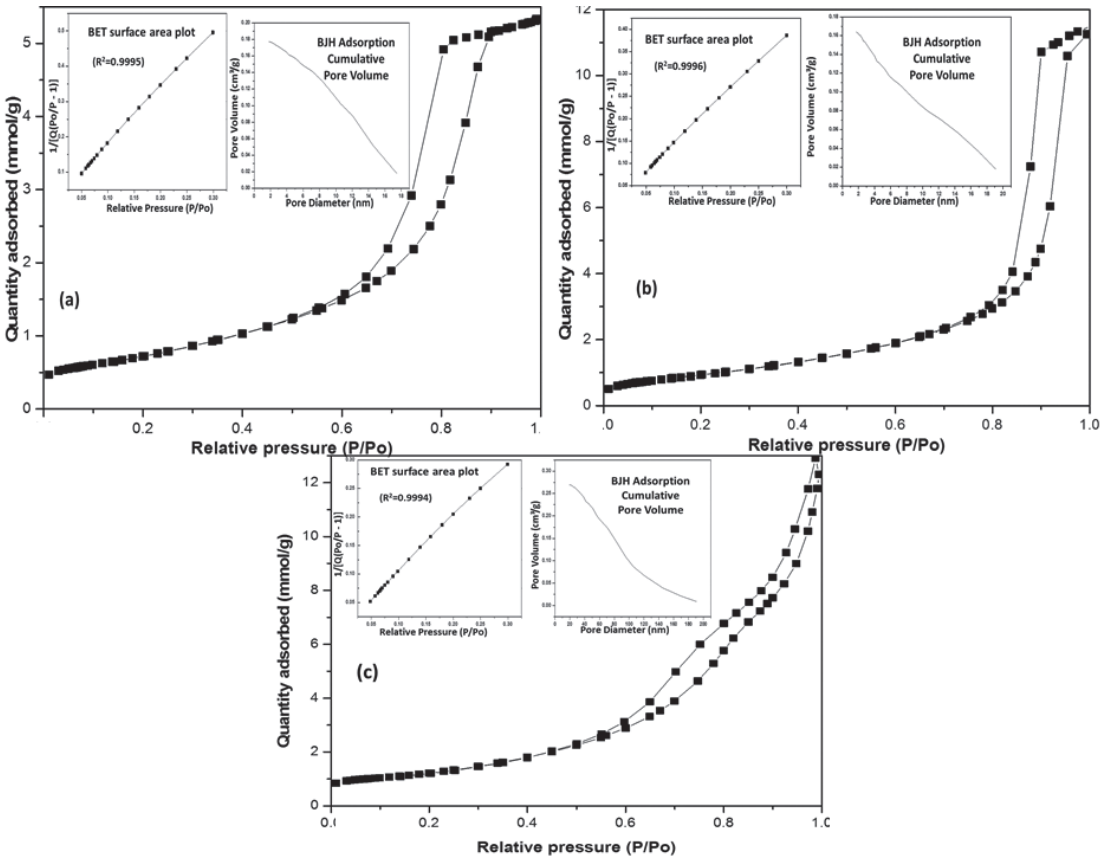

Figure 2: Nitrogen adsorption-desorption isotherm, BET plot (inset) and BJH adsorption cumulative pore volume curve (inset) for (a) C/TiO_2, (b) H/TiO_2, (c) C,H/TiO_2.

3 Results and Discussion

3.1 *Surface analysis*

Surface properties are essential components of photocatalyst characterization. Figure 2 shows the nitrogen adsorption-desorption isotherm, BET surface area plot (left inset) and BJH adsorption cumulative pore volume curve (right inset) for the C,H/TiO_2, H/TiO_2 and C/TiO_2 used in this study. Based on the IUPAC classification the catalysts exhibit a type IV isotherm. This can be readily observed from the hysteresis loops and obvious condensation/evaporation steps within partial pressure range of 0.6 to 0.9 [37]. The hysteresis loops confirm the presence of mesoporous structure in the synthesized photocatalysts [38].

The surface area and pore volume of the catalysts were estimated using Brunauer-Emmett-Teller (BET) and Barrett-Joyner-Halenda (BJH) methods. The HDMA-derived catalyst H/TiO_2 has a surface area of 77.5 m^2/g, a pore volume of 0.372 cm^3/g and a pore size of 19.2 nm while those properties of C/TiO_2 are 53.1 m^2/g, 0.146 cm^3/g and 11.01 nm respectively. Even though the pore volume and pore size of C,H/TiO_2 particles decrease to 0.295 cm^3/g and 11.9 nm respectively, the surface area increases to 99.5 m^2/g due to the beneficial effect of chitosan-HDMA bi-template. The surface area and pore volume of the C,H/TiO_2 are higher than those reported by Chang et al. for an anatase TiO_2 derived using diblock copolymer template (89 m^2/g) [39] and an Ag-S/TiO_2 synthesized using polyethylene glycol as template (68 m^2/g) [40].

3.2 *Structural and compositional analysis*

The crystalline structures of the synthesized W/TiO_2,

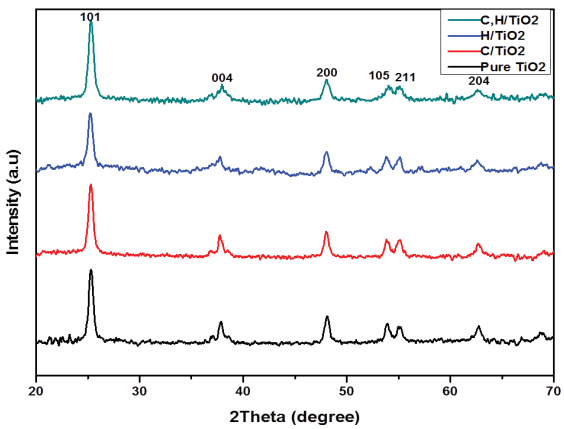

Figure 3: The XRD patterns of the synthesized catalysts.

C/TiO_2, H/TiO_2 and $C,H/TiO_2$ photocatalysts were recorded on XRD (Figure 3) and compared with JCPDS-21-1272 and JCPDS-21-1276 patterns. All the experimental patterns revealed pure anatase phase with XRD peaks at 2θ (and planes) as 25.23° (101), 37.69° (004), 48.04° (200), 53.96° (105), 55.05° (211), and 62.73° (204). Moreover, according to the Scherrer equation, the average crystal sizes of W/TiO_2, C/TiO_2, H/TiO_2, and $C,H/TiO_2$ were 17.18, 16.99, 14.68, and 12.78 nm, respectively. The results showed that the average crystal size decreases as templates are applied separately or combined. This means that the templates not simply functions as the meso-structure directing agents, but may also suppress the growth of TiO_2 crystals during the calcination.

To examine the influence of the chitosan and HDTMA templates employed separately or as bi-template on the titania morphology and to further depict the meso-structures obtained, SEM images of W/TiO_2, C/TiO_2, H/TiO_2 and $C,H/TiO_2$ were collected and are shown in Figure 4. It can be seen from the figure, the W/TiO_2 shows only the aggregates of titania crystals. In contrast, meso-structures can be observed for C/TiO_2, H/TiO_2 and $C,H/TiO_2$ catalyst due to the present of struts as depicted by Figure 4(b), (c), and (d) respectively. The density of these structures is more in H/TiO_2

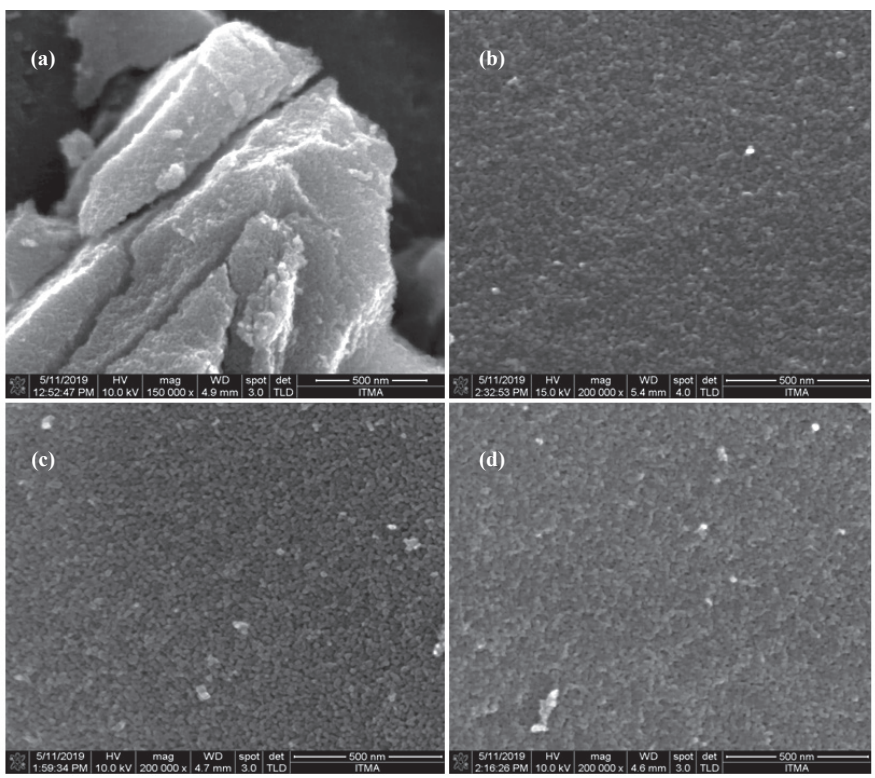

Figure 4: The FE-SEM images of (a) W/TiO_2, (b) C/TiO_2, (c) H/TiO_2, and (d) $C,H/TiO_2$.

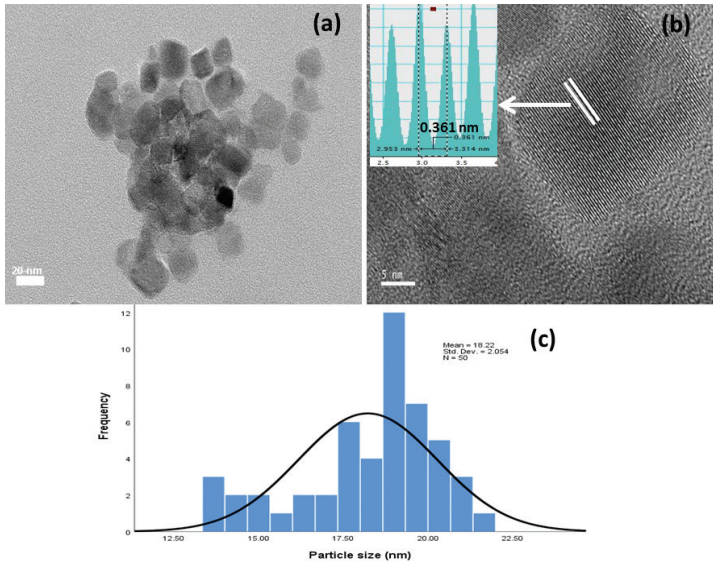

Figure 5: The TEM images of C/TiO_2 at different magnifications (a) and (b), and size distribution curve (c).

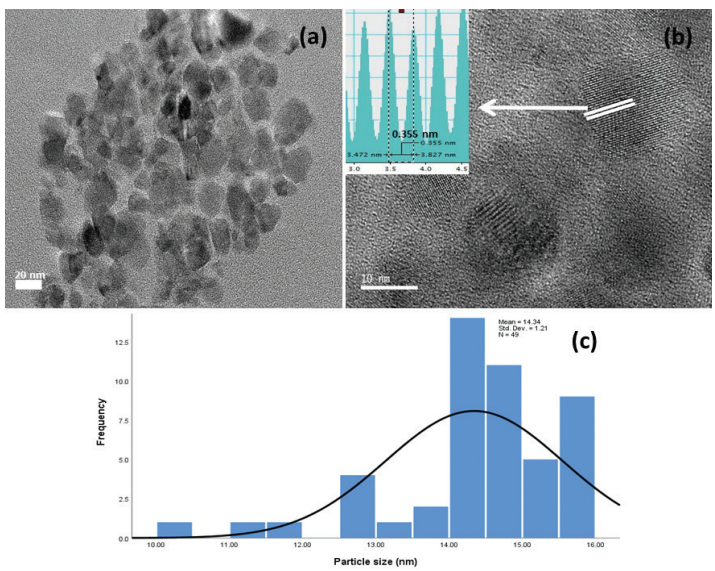

Figure 6: The TEM images of H/TiO_2 at different magnifications (a) and (b), and size distribution curve (c).

than in C/TiO_2, with the least in $C,H/TiO_2$, and inconsistent with pore sizes. It has been shown that these pore sizes are governed by the decomposition of the templates during the calcination process [34]. As such, the order of average pore size is $H/TiO_2 > C,H/TiO_2 > C/TiO_2$.

The morphology of the synthesized catalysts was recorded on TEM. Figures 5–7 show TEM images and size distribution curve of C/TiO_2, H/TiO_2 and $C,H/TiO_2$, respectively. All of these materials exhibit a cube-like shape. The C/TiO_2, H/TiO_2 and $C,H/TiO_2$ powders have average particle sizes of 18.22 nm [Figure 5(b)], 14.34 nm [Figure 6(b)], and 12.80 nm [Figure 7(b)], respectively. It can be seen that the use of bi-template results in a comparatively tinier material ($C,H/TiO_2$), in terms of particle size than

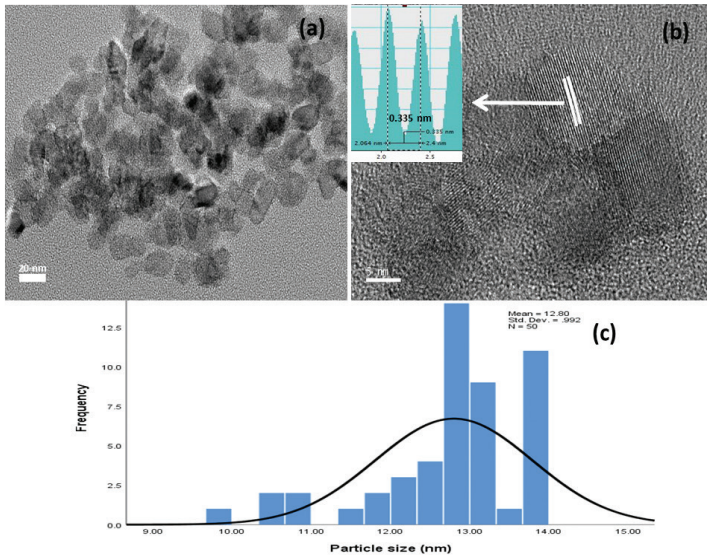

Figure 7: The TEM images of C,H/TiO_2 at different magnifications (a) and (b), and size distribution curve (c).

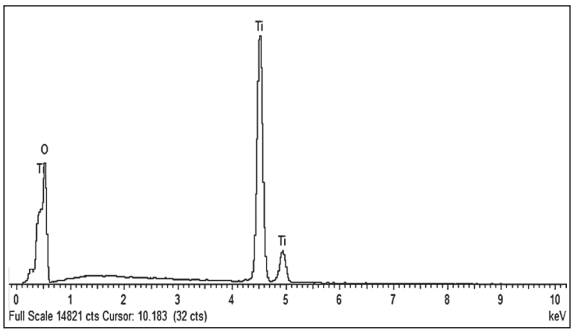

Figure 8: The EDX analysis of C,H/TiO_2.

TiO_2 produced using single templates such as lignin (30–80 nm) [22], polyethylene glycol (20 nm) [40], P123 (40 nm) [41] and cellulose (10–30 nm) [42]. The reduction in particle size when using the bi-template can be attributed to the successive dispersion and separation of the TiO_2 precursor ($Ti(OH)_4$) within the chitosan and HDTMA structure which could effectively prevent nanoparticle aggregations during calcination. The insets of the Figures 5(c), 6(c), and 7(c) reveal the polycrystalline structures of C/TiO_2, H/TiO_2 and C,H/TiO_2, with interplanar spaces of 0.361, 0.355 and 0.335 nm respectively, which correspond to the (101) crystal facets of anatase TiO_2 [43].

To perform elemental analysis of the synthesized catalysts, EDX spectra of C,H/TiO_2 were acquired (Figure 8). The EDX spectra show the characteristic peaks of Ti (55.19%) and O (44.54%), confirming the elements in the synthesized TiO_2.

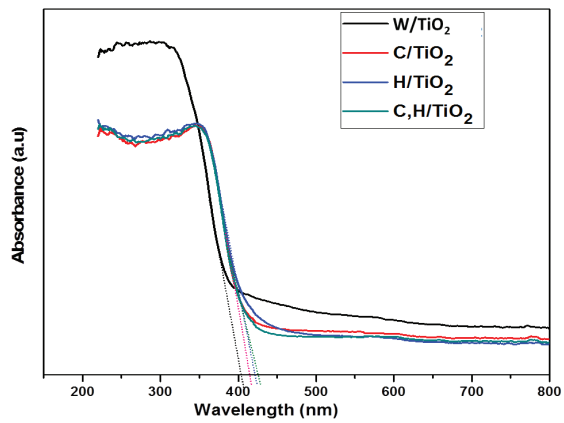

Figure 9: UV-vis spectra of the synthesized materials.

3.3 *Band gap analysis*

The optical absorptions of the synthesized photocatalysts were studied by UV-vis analysis. Figure 9 shows the UV–vis absorption spectra of the synthesized TiO_2 powders. Their band gap energies (E_g) were estimated from the absorption spectra using Equation (4) [40].

$$E_g = \frac{hc}{\lambda} \quad (4)$$

Where E_g is the band-gap energy (eV), h is Planck's constant, and c is the velocity of light. Moreover, λ is the wavelength (nm) corresponding to the intersection point of the horizontal axis and the tangent to the absorbance curve of the spectra (at the point where the slope of the absorbance curve suddenly varies). The calculated band-gap energies of W/TiO_2, C/TiO_2, H/TiO_2 and C,H/TiO_2 were 3.08, 2.99, 2.94 and 2.92 eV, respectively. These results illustrate that the band-gap energy of the W/TiO_2 without template decreased from 3.08 to 2.99 eV for C/TiO_2 when chitosan was used as the template and 2.94 for H/TiO_2 when HDMA was used. It was found that the band-gap energy further decreased to 2.92 for the C,H/TiO_2 catalyst obtained by using two templates.

The results reveal that lowest band gap energy of 2.92 eV was obtained for C,H/TiO_2 catalyst which is comparably lower than the meso-TiO_2 prepared using triblock Pluronic P123 as template [41], [44], polyethylene glycol as template [45] and phenoxyacetic acid as template [46]. The decrease in the band gap energy value may be due to size reduction of the C,H/TiO_2 photocatalyst [46], [47]. It was strongly believed that a decreased band gap energy yields more redox power for production of photogenerated electron-hole pairs and strongly reduces recombination effect, which overall contributes to increase the photocatalytic performance of photomaterials [48].

3.4 *Thermal analysis*

Because polymers and large organic molecules undergo several changes when subjected to a high temperature, releasing gases and liquids of different shapes, colors and molecular weights [49], the residual content of templates and the stability of the TiO_2 phase were examined using thermogravimetric analysis (TGA) and differential thermal analysis (DTA). The DTA curve of the C,H/TiO_2 precursor [Figure 10(a)] shows three endothermic peaks. The first endothermic phenomenon visible at 63.43°C is due to the release of adsorbed water molecules by evaporation [50] while the second endothermic phenomenon at 320.76°C is due to the thermal decomposition of alkylammonium ions physically interacting via van der-Waals forces with the precursor or their partners [50], [51]. The third endothermic phenomenon shows at 369.14°C and is linked to depolymerization and decomposition

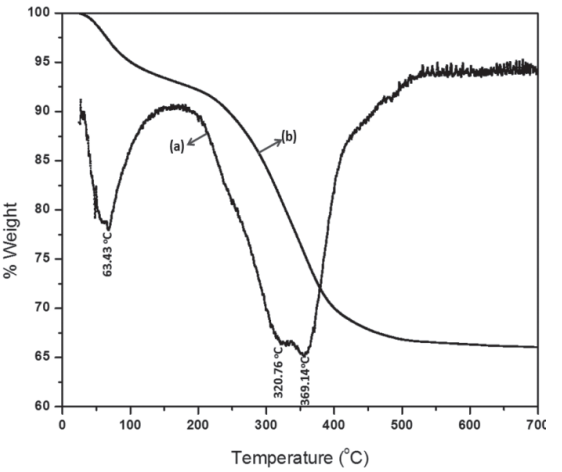

Figure 10: The TGA/DTA thermograms of the C,H/TiO_2 precursor.

of the chitosan [52], [53]. These phenomena confirm the suitability of the calcination temperature (500°C for 4 h) for the synthesis of C,H/TiO_2 as used in this study. These observations are affirmed by the TGA curve depicted in Figure 10(b). From the TGA curve, a weight loss was observed between 70–100°C, 200–338°C and 338–500°C which correspond to the evaporation of volatile and physically adsorbed water, decomposition of chitosan and HDTMA, respectively. No weight loss was observed above 500°C, indicating that the templates decomposed completely around this temperature leaving behind only the stable meso-TiO_2. The thermogram also shows the stability of the TiO_2 anatase phase up to 700°C. Generally, a lower thermal stability of the TiO_2 phase is undesirable, especially for the use of TiO_2 as photocatalyst since the transformation to rutile, which has long been considered to have lesser photocatalytic activity, may take place [54].

3.5 *Photocatalytic performance*

To evaluate the photocatalytic performance of the as-synthesized catalysts, photodegradation of MO was performed under UV photolysis, in the dark with TiO_2 photocatalyst and under photocatalytic regime in presence of W/TiO_2, C/TiO_2, H/TiO_2 and C,H/TiO_2. The results are displayed in Figure 11. The corresponding photocatalytic performance of are 77.46, 80.85, 89.72 and 98.1%, respectively, which reveals the superiority of C,H/TiO_2. The superior performance of the latter can

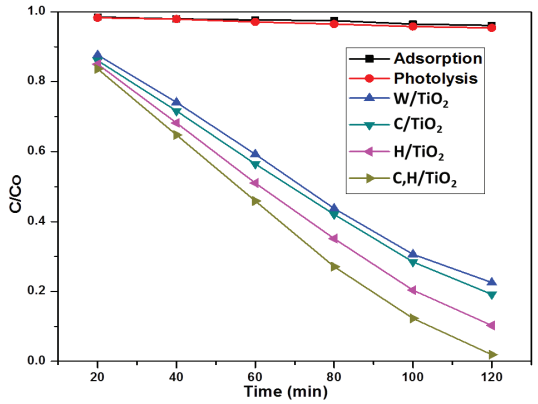

Figure 11: Photocatalytic degradation of profile of MO (20 mg/L) over synthesized photocatalysts (0.8 g/L).

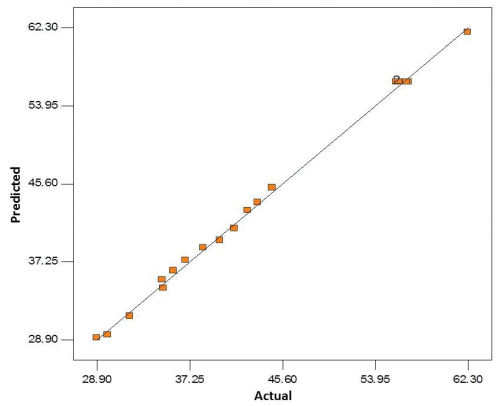

Figure 12: Plot of the variation of experimental degradation efficiency with predicted values.

attributed to the improved particle size, pore volume and surface area in this catalyst, and shortest band gap, which cause better surficial adsorption of dye molecules and their penetration through the channels of the catalyst [22], [55]. In both photolytic and dark adsorption systems, less than 5% of MO disappears, indicating that the removal of MO under UV/TiO_2 photocatalysis is almost entirely based on photocatalytic phenomenon.

The degradation of MO over the synthesized photocatalysts were found to follow pseudo-first-order kinetics represented by Equation (5).

$$\ln \frac{[MO]_o}{[MO]_t} = kt \quad (5)$$

Where $[MO]_t$ and $[MO]_o$ are the concentrations (mg/L) at time t and when $t = 0$, respectively, and k is the apparent reaction rate constant (min^{-1}). A plot of $\ln([MO]_o/[MO]_t)$ versus t gave a straight line with slope = k and R-square values > 0.9 as shown in Figure 12. The rate constants for degradation over W/TiO_2, C/TiO_2, H/TiO_2 and C,H/TiO_2 are 0.0112 min^{-1}, 0.0122 min^{-1}, 0.0158 min^{-1} and 0.0173 min^{-1}, respectively. It can be seen from the results that C,H/TiO_2 derived from the combined two templates offered the highest rate constant 0.0173 min^{-1}. This value is higher compared with those reported in many literature [6], [56], [57].

3.6 *Optimisation*

The interactive impacts of three independent variables (TiO_2 loading, initial concentration of MO and pH) on the degradation of MO were investigated using the central composite factorial design. To develop the mathematical relationship between the response and the independent process variables, the experimental degradation efficiency values (D%) were processed, giving a cubic polynomial model with considerably low standard deviation of 0.77 and PRESS value of 161.33 as shown in Equation (5)

$$D\ (\%) = 56.49 + 4.88[TiO_2] + 2.79[MO] + 1.88(pH) - 6.91[TiO_2]^2 - 7.21[MO]^2 - 3.85(pH)^2 + 0.94[MO](pH) - 1.19[TiO_2]^3 - [4.07(pH)^3 - 0.63[MO][TiO_2]^2 \quad (6)$$

Each coefficient of the variable in Equation (6) corresponds to the change in mean degradation efficiency per unit increase in the associated independent factor when the other factor is held constant, which predicts the degradation efficiencies presented in Table 2. It can be seen from the tables that the experimental and predicted D% correlate well and this has been supported by linear normal plot of residuals. The normal probability plot showed the residuals following a normal distribution, in which the points will follow a straight line as recommended [36], [58]. This observation is further supported by parity plot in Figure 12 which shows the distribution of the experimental degradation efficiencies with predicted responses. The linear distribution of both values is an indication of agreement between the experimental results with the predicted ones.

The statistical significance of the CCD model was assessed by the analysis of variance, ANOVA (Table 3).

Table 2: The central composite design matrix and the value of the response function (D%)

Run	TiO_2 (g/L)	[MO] (mg/L)	pH	Experimental D%	Predicted D%
1	0.8	30	5.5	41.3	40.81
2	0.4	20	5.5	34.9	34.41
3	0.8	20	5.5	55.9	56.49
4	0.6	15	4.0	35.8	35.81
5	0.8	20	2.5	62.3	61.81
6	0.8	20	5.5	56.2	56.49
7	0.8	20	5.5	57.0	56.49
8	1.0	25	7.0	43.4	43.13
9	1.2	20	5.5	40.0	39.51
10	0.8	20	8.5	29.9	29.41
11	1.0	15	4.0	42.5	43.18
12	0.8	20	5.5	56.1	56.49
13	1.0	15	7.0	36.9	36.93
14	1.0	25	4.0	44.7	45.63
15	0.8	20	5.5	56.8	56.49
16	0.6	25	4.0	38.5	38.26
17	0.6	15	7.0	28.9	29.56
18	0.6	25	7.0	34.8	35.76
19	0.8	10	5.5	31.9	31.41
20	0.8	20	5.5	56.8	56.49

The high F-value of 369.97, probability > F of less than 0.05 and insignificant lack of fit, as obtained for the model are not influenced at 95% confidence level. Furthermore, statistical measures revealed the suitability of the model to navigate the design space. The R^2 value was 0.9976, with only about 0.24% the variation for MO degradation efficiency not explained by the model. In a system like this, with different number of independent variables, adjusted R^2 (Adj-R^2) is more suitable for evaluating the model goodness of fit [35]. The obtained Adj-R^2 value was 0.9949 which is also closed to 1 and the minimum adequate precision (56.953) is a value well above 4.

In order to validate the obtained results by the model and to confirm the model competence for predicting MO degradation, three experiments were conducted. From the experiments, 62.31 ± 0.48% average MO dye degradation efficiency was obtained which is very close in all respect to value based on the model (61.81%).

In this study, a maximum experimental MO percentage degradation of 62.3% was attained after treatment for 60 min, under optimum conditions of H,C/TiO_2 catalyst dosage of 0.8 gL^{-1}, initial MO concentration of 20 mgL^{-1} and pH of 2.5. To achieve maximum MO percentage degradation, numerical optimization was further conducted using a combination

Table 3: ANOVA for cubic models

Source	Sum of Square	DF	Mean Square	F-value	Prob>F	Remarks
Model	2177.05	10	217.70	369.97	< 0.0001	Significant
A	67.52	1	67.52	114.74	< 0.0001	
B	44.18	1	44.18	75.08	< 0.0001	
C	10.09	1	10.09	17.14	0.0025	
A^2	687.37	1	687.37	1168.14	< 0.0001	
B^2	748.50	1	748.50		< 0.0001	
C^2	213.40	1	213.40	1272.01	< 0.0001	
BC	7.03	1	7.03		0.0072	
A^3	15.62	1	15.62	362.65	0.0006	
C^3	183.68	1	183.68	11.95	< 0.0001	
A^2B	1.32	1	1.32	26.55	0.1678	
A^2C	0.000	0		312.14		
AB^2	0.000	0		2.25		
AC^2	0.000	0				
B^2C	0.000	0				
BC^2	0.000	0				
Residual	5.30	9	0.59			
Lack of Fit	4.26	4	1.07		0.0507	Not significant
Pure Error	1.03	5	0.21			
Cor Total	2182.34	19		5.16		

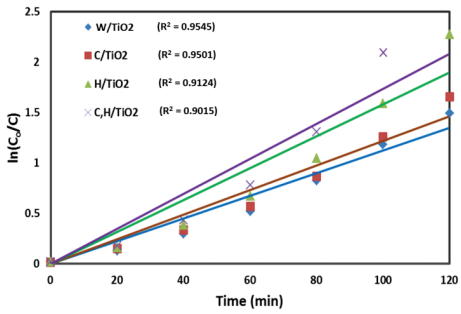

Figure 13: Pseudo-first-order graph of MO photocatalytic degradation.

of the three parameters, the TiO_2 dosage, the initial concentration of MO and pH. A maximum percentage degradation of 62.3554% was obtained at TiO_2 value of 0.852 gL^{-1}, [MO] value of 20.01 mg/L and pH value of 2.5 with desirability factor 1 (Figure 13).

3.7 *Response surface analysis*

The interactive effect of the independent variables on the MO degradation efficiency was depicted by 3D surface (Figure 14), in which one variable was kept constant while the other two were varied. As observed from Figure 14(a), the MO degradation efficiency increases with TiO_2 concentration up to 1 g/L, likely due to increased hydroxyl and superoxide radical generation [59]. Subsequently, the degradation efficiency decreases with further increase in TiO_2 perhaps due to the increase in opacity. The influence of pH vis-à-vis TiO_2 concentration or MO concentration is depicted by Figure 14(b) and (c), respectively. There is increase in degradation at acidic pH levels due to the predominance of protonated form of the MO, and strong adsorption onto the TiO_2 catalyst [Figure 14(b)]. On the other hand, the more the MO amounts were increased, the more degradation is affected by inhibitive effect on light penetration and catalyst site saturation [60]

4 Conclusions

A stable, mesoporous TiO_2 photocatalyst has been successfully synthesized by templating with a combined chitosan-HDTMA assisted sol-gel method. This catalyst exhibits anatase structure, and consequently high photocatalytic activity.

Acknowledgments

The authors acknowledge the Universiti Putra Malaysia (UPM) where part of this work was conducted under the Mobility Program. Abubakar Hamisu gratefully acknowledges his sponsorship for PhD and benchwork by the Kano State University of Technology through the Tertiary Education Trust Fund (TETFUND).

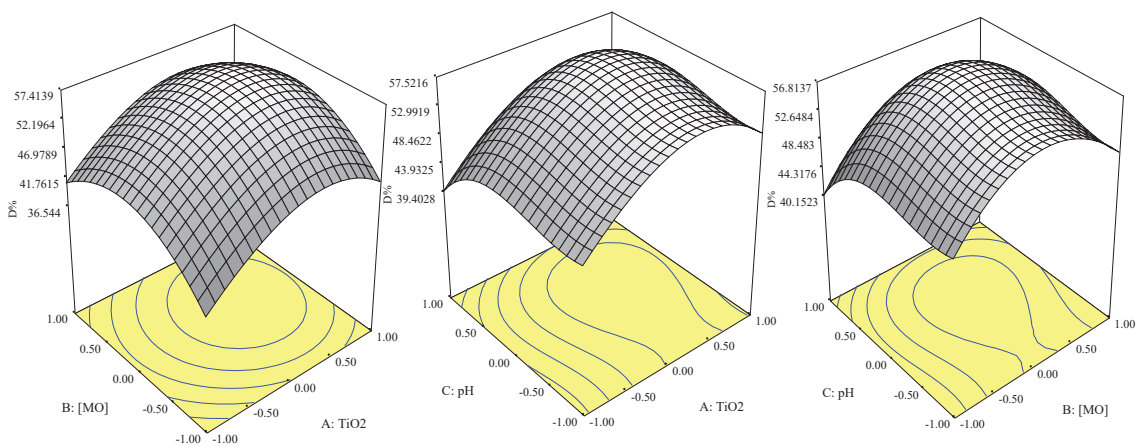

(a) (b) (c)

Figure 14: The 3D response surface of MO dye degradation efficiency (D%) as a function (a) TiO_2 catalyst loading and initial MO concentration, (b) pH level and TiO_2 catalyst loading and (c) initial MO concentration and pH level.

References

[1] J. Yang, J. Du, X. Li, Y. Liu, C. Jiang, W. Qi, K. Zhang, C. Gong, R. Li, and M. Luo, "Highly hydrophilic TiO_2 nanotubes network by alkaline hydrothermal method for photocatalysis degradation of methyl orange," *Nanomaterials*, vol. 9, no. 4, p. 526, 2019, doi: 10.3390/nano9040526.

[2] R. Saravanan, D. Manoj, J. Qin, M. Naushad, F. Gracia, A. F. Lee, M. M. Khan, and M. Gracia-Pinilla, "Mechanothermal synthesis of Ag/TiO_2 for photocatalytic methyl orange degradation and hydrogen production," *Process Safety and Environmental Protection*, vol 120, pp. 339–347, 2018, doi: 10.1016/j.psep.2018.09.015.

[3] M. R. Awual, M. M. Hasan, M. A. Khaleque, and M. C. Sheikh, "Treatment of copper (II) containing wastewater by a newly developed ligand based facial conjugate materials," *Chemical Engineering Journal*, vol. 288, pp. 368–376, 2016.

[4] M. R. Awual, M. M. Hasan, M. Naushad, H. Shiwaku, and T. Yaita, "Preparation of new class composite adsorbent for enhanced palladium (II) detection and recovery," *Sensors and Actuators B*, vol. 209, pp. 790–797, 2015, doi: 10.1016/j.snb.2014.12.053.

[5] M. Gunay, "Eco-friendly textile dyeing and finishing," *Intechopen*, 2013, doi: 10.5772/3436.

[6] L. Bai, S. Wang, Z. Wang, E. Hong, Y. Wang, C. Xia, and B. Wang, "Kinetics and mechanism of photocatalytic degradation of methyl orange in water by mesoporous Nd-TiO_2-SBA-15 nanocatalyst," *Environmental Pollution*, vol. 248, pp. 516–525, 2019, doi: 10.1016/j.envpol.2019.02.052.

[7] W. Buraso, V. Lachom, P. Siriya, and P. Laokul, "Synthesis of TiO_2 nanoparticles via a simple precipitation method and photocatalytic performance," *Materials Research Express*, vol 5, no. 11, p. 115003, 2018, doi: 10.1088/2053-1591/aadbf0.

[8] J. Saien and Z. Mesgari, "Photocatalytic degradation of methyl orange using hematoporphyrin/N- doped TiO_2 nanohybrids under visible light: Kinetics and energy consumption," *Applied Organomettalic Chemistry*, vol. 31, no. 11, p. ee3755, 2017, doi: 10.1002/aoc.3755.

[9] E. Kusiak-Nejman and A. W. Morawski, "TiO_2/graphene-based nanocomposites for water treatment: A brief overview of charge carrier transfer, antimicrobial and photocatalytic performance," *Applied Catalysis B: Environmental*, vol. 253, pp. 179–186, 2019, doi: 10.1016/j.apcatb.2019.04.055.

[10] S. Mallakpour and E. Nikkhoo, "Surface modification of nano-TiO_2 with trimellitylimido-amino acid-based diacids for preventing aggregation of nanoparticles," *Advanced Powder Technology*, vol. 25, pp. 348–353, 2014. doi: 10.1016/j.apt.2013.05.017.

[11] N. Raza, W. Raza, H. Gul, M. Azam, J. Lee, K. Vikrant, and K. H. Kim, "Solar-light active silver phosphate/titanium dioxide/silica heterostructures for photocatalytic removal of organic dye," *Journal of Cleaner Production*, vol. 254, p. 120031, 2020, doi: 10.1016/j.jclepro.2020.120031.

[12] D. Chen , Y. Cheng , N. Zhou , P. Chen , Y. Wang, K. Li, S. Huo, P. Cheng, P. Peng, R. Zhang, L. Wang, H. Liu, Y. Liu, and R. Ruan, "Photocatalytic degradation of organic pollutants using TiO_2-based photocatalysts: A review," *Journal of Cleaner Production*, vol. 268, p. 121725, 2020, doi: 10.1016/j.jclepro.2020.121725.

[13] M. Humayun, F. Raziq, A. Khan, and W. Luo, "Modification strategies of TiO_2 for potential applications in photocatalysis: A critical review" *Green Chemistry Letters and Reviews*, vol. 11, pp. 86–102, 2018, doi: 10.1080/17518253.2018.1440324.

[14] M. R. Al-Mamun, S. Kader, M. S. Islam, M. Z. H. Khan, M. R. Al-Mamun, S. Kaderb, M. S. Islam, and M. Z. H. Khan, "Photocatalytic activity improvement and application of UV-TiO_2 photocatalysis in textile wastewater treatment: A review" *Journal of Environmental Chemical Engineering*, vol. 7, p. 103248, 2019, doi: 10.1016/j.jece.2019.103248.

[15] D. G. Shchukin, J. H. Schattka, M. Antonietti, and R. A. Caruso, "Photocatalytic properties of porous metal oxide networks formed by nanoparticle infiltration in a polymer gel template," *Journal of Physical Chemistry B*, vol. 107, no. 4, pp. 952–957, 2003. doi: 10.1021/jp026929i.

[16] L. H. Kao, T. C. Hsu, and K. K. Cheng, "Novel synthesis of high-surface-area ordered mesoporous TiO_2 with anatase framework for photocatalytic

applications," *Journal of Colloid and Interface Science*, vol. 341, no. 2, pp. 359–365, 2010, doi: 10.1016/j.jcis.2009.09.058.

[17] D. Grosso, G. J. d. A. A. Soler-Illia, E. L. Crepaldi, F. Cagnol, C. Sinturel, A. Bourgeois, A. Brunet-Bruneau, H. Amenitsch, P. A. Albouy, and C. Sanchez, "Highly porous TiO_2 anatase optical thin films with cubic mesostructure stabilized at 700°C," *Chemistry of Materials*, vol. 15, no. 24, pp. 4562–4570, 2003, doi: 10.1021/cm031060h.

[18] D. M. Antonelli and J. Y. Ying, "Synthesis of hexagonally packed mesoporous TiO_2 by a modified sol–gel method," *Angewandte Chemie, International Edition in English*, vol. 34, no. 18, pp. 2014–2017, 1995, doi: 10.1002/anie.199520141.

[19] T. Preethi, B. Abarna, and G. R. Rajarajeswari, "Influence of chitosan–PEG binary template on the crystallite characteristics of sol–gel synthesised mesoporous nanotitania photocatalyst," *Applied Surface Science*, vol. 317, pp. 90–97, 2014, doi: 10.1016/j.apsusc.2014.10.002.

[20] J. Ramos, I. Mejia, J. Murphy, M. Quevedo, P. Garcia, and C. Martinez, "Synthesis of titanium oxide nanoparticles using DNA-complex as template for solution-processable hybrid dielectric composites," *Journal of Alloys and Compounds*, vol. 643, no. 1, pp. S84–S89, 2015, doi: 10.1016/j.jallcom.2014.09.201.

[21] K. Ö. Hamaloğlu, B. Çelebi, E. Sağ, and A. Tuncel, "A new method for the synthesis of monodisperse-porous titania microbeads by using polymethacrylate microbeads as template," *Microporous and Mesoporous Materials*, vol. 207, pp. 17–26, 2015, doi: 10.1016/j.micromeso.2015.01.001.

[22] X. Chen, D.-H. Kuo, D. Lu, Y. Hou, and Y.-R. Kuo, "Synthesis and photocatalytic activity of mesoporous TiO_2 nanoparticle using biological renewable resource of un-modified lignin as a template," *Microporous and Mesoporous Materials*, vol. 223, no. 145–151, 2016, doi: 10.1016/j.micromeso.2015.11.005.

[23] E. Ovodok, H. Maltanava, S. Poznyak, M. Ivanovskaya, A. Kudlash, N. Scharnagl, and J. Tedim, "Sol-gel template synthesis of mesoporous carbon-doped TiO_2 with photocatalytic activity under visible light," *Materials Today: Proceedings*, vol. 5, no. 9, pp. 17422–17430, 2018, doi: 10.1016/j.matpr.2018.06.044.

[24] B. Niu, X. Wang, K. Wu, X. He, and R. Zhang, "Mesoporous titanium dioxide: Synthesis and applications in photocatalysis, energy and biology," *Materials*, vol. 11, no. 10, p. 1910, 2018, doi: 10.3390/ma11101910.

[25] A. Hamisu, U. I. Gaya, and A. H. Abdullah, "A novel poly (vinyl alcohol) post-precipitation template synthesis and property tuning of photoactive mesoporous nano-TiO_2," *Physical Chemistry Research*, vol. 8, no. 2, pp. 281–295, 2020, doi: 10.22036/PCR.2020.210668.1704.

[26] W. Li, Z. Wu, J. Wang, A. A. Elzatahry, and D. Zhao, "A perspective on mesoporous TiO_2 materials," *Chemistry of Materials*, vol. 26, no. 1, pp. 287–298, 2013, doi: 10.1021/cm4014859.

[27] M. E. Davis, "Ordered porous materials for emerging applications," *Nature*, vol. 417, no. 813–821, 2002, doi: 10.1038/nature00785.

[28] T. P. Braga, E. C. C. Gomes, A. F. de Sousa, N. L. V. Carreño, E. Longhinotti, and A. Valentini, "Synthesis of hybrid mesoporous spheres using the chitosan as template," *Journal of Non-Crystalline Solids*, vol. 355, no. 14–15, pp. 860–866, 2009, doi: 10.1016/j.jnoncrysol.2009.04.005.

[29] Z. Abou-Gamra and M. Ahmed, "Synthesis of mesoporous TiO_2–curcumin nanoparticles for photocatalytic degradation of methylene blue dye," *Journal of Photochemistry and Photobiology B*, vol. 160, no. 134–141, 2016, doi: 10.1016/j.jphotobiol.2016.03.054.

[30] T. Witoon, M. Chareonpanich, and J. Limtrakul, "Synthesis of bimodal porous silica from rice husk ash via sol–gel process using chitosan as template," *Materials Letters*, vol. 62, no. 10–11, pp. 1476–1479, 2018, doi: 10.1016/j.matlet.2007.09.004.

[31] K. C. L. Khang, M. H. M. Hatta, S. L. Lee, and L. Yuliati, "Photocatalytic removal of phenol over mesoporous ZnO/TiO_2 composites," *Jurnal Teknologi*, vol. 80, no. 2, pp. 153–160, 2018, doi: 10.11113/jt.v80.11209.

[32] G. He, J. Zhang, Y. Hu, Z. Bai, and C. Wei, "Dual-template synthesis of mesoporous TiO_2 nanotubes with structure-enhanced functional photocatalytic performance," *Applied Catalysis, B*, vol. 250, pp. 301–312, 2019, doi: 10.1016/j.apcatb.2019.03.027.

[33] P. Messina, M. A. Morini, and P. C. Schulz, "Siliceous mesoporous material templated with hexadecyltrimethylammonium bromide–sodium dehydrocholate mixed micelles," *Colloid and Polymer Science*, vol. 282, pp. 1063–1066, 2004, doi: 10.1007/s00396-003-1034-7.

[34] J. Wei, Z. Sun, W. Luo, Y. Li, A. A. Elzatahry, A. M. Al-Enizi, Y. Deng, and D. Zhao, "New insight into the synthesis of large-pore ordered mesoporous materials," *Journal of the American Chemical Society*, vol. 139, pp. 1706–1713, 2017, doi :10.1021/jacs.6b11411.

[35] U. I. Gaya, A. H. Abdullah, Z. Zainal, and M. Z. Hussein, "Photocatalytic treatment of 4-chlorophenol in aqueous ZnO suspensions: Intermediates, influence of dosage and inorganic anions," *Journal of Hazardous Materials*, vol. 168, no. 1, pp. 57–63, 2009, doi: 10.1016/j.jhazmat. 2009.01.130.

[36] A. H. Jawad, A. F. M. Alkarkhi, and N. S. A. Mubarak, "Photocatalytic decolorization of methylene blue by an immobilized TiO_2 film under visible light irradiation: Optimization using response surface methodology (RSM)," *Desalination and Water Treatment*, vol. 56, no. 1, pp. 161–172, 2015, doi: 10.1080/19443994.2014.934736.

[37] L. Cano-Casanova, A. Amorós-Pérez, M. Ouzzine, M. A. Lillo-Ródenas, and M. C. Román-Martínez, "One step hydrothermal synthesis of TiO_2 with variable HCl concentration: Detailed characterization and photocatalytic activity in propene oxidation," *Applied Catalysis, B*, vol. 220, pp. 645–653, 2018, doi: 10.1016/j.apcatb.2017.08.060.

[38] M. M. Abbad, A. A. H. Kadhum, A. B. Mohamad, M. S. Takriff, and K. Sopian, "Synthesis and catalytic activity of TiO_2 nanoparticles for photochemical oxidation of concentrated chlorophenols under direct solar radiation," *International Journal of Electrochemical Science*, vol. 7, pp. 4871–4888, 2012, doi: 10.1.1.470.8294.

[39] J. Chang, W. Zhang, and C. Hong, "Template-directed fabrication of anatase TiO_2 hollow nanoparticles and their application in photocatalytic degradation of methyl orange," *Chinese Journal of Chemistry*, vol. 35, no. 6, pp. 1016–1022, 2017, doi: 10.1002/cjoc.201600890.

[40] M. Feilizadeh, M. Vossoughi, S. M. E. Zakeri, and M. Rahimi, "Enhancement of efficient Ag–S/TiO_2 nanophotocatalyst for photocatalytic degradation under visible light," *Industrial & Engineering Chemistry Research*, vol. 53, no. 23, pp. 9578–9586, 2014, doi: 10.1007/s11164-013-1519-z.

[41] M. A. A. Sadatlu and N. Mozaffari, "Synthesis of mesoporous TiO_2 structures through P123 copolymer as the structural directing agent and assessment of their performance in dye-sensitized solar cells," *Solar Energy*, vol. 133, no. 24–34, 2016, doi: 10.1016/j.solener.2016.03.056.

[42] X. Chen, D. H. Kuo, and D. Lu, "N-doped mesoporous TiO_2 nanoparticles synthesized by using biological renewable nanocrystalline cellulose as template for the degradation of pollutants under visible and sun light," *Chemical Engineering Journal*, vol. 295, pp. 192–200, 2016, doi: 10.1016/j.cej.2016.03.047.

[43] T. Huang, S. Mao, J. Yu, Z. Wen, G. Lu, and J. Chen, "Effects of N and F doping on structure and photocatalytic properties of anatase TiO_2 nanoparticles," *RSC Advances*, vol. 3, pp. 16657–16664, doi: 10.1039/C3RA42600A.

[44] T. Diaconu, M. Ciobanu, G. Petcu, D. Culita, S. Preda, J. Pandele-Cusu, M. Mureseanu, and V. Parvulescu, "Cerium modified mesoporous TiO_2 photocatalyst obtained by sol-gel method," *Revue Roumaine de Chimie*, vol. 63, no. 5–6, pp. 467–474, 2018.

[45] A. Maddu, R. Purwati, and M. Kurniat, "Effects of poly-ethylene glycol (PEG) template on structural and optical properties of nanocrystalline titanium dioxide (TiO_2) films," *Journal of Ceramic Processing Research*, vol. 17, pp. 360–364, 2016, doi: 10.1380/ejssnt.2012.103.

[46] P. V. Bakre and S. Tilve, "Direct access to highly crystalline mesoporous nano TiO_2 using sterically bulky organic acid templates," *Journal of Physics and Chemistry of Solids*, vol. 116, pp. 234–240, 2018, doi: 10.1016/j.jpcs.2018.01.043.

[47] K. Thamaphat, P. Limsuwan, and B. Ngotawornchai, "Phase characterization of TiO_2 powder by XRD and TEM," *Kasetsart Journal (Natural Science)*, vol. 42, no. 5, pp. 357–361, 2008,doi: 10.1016/j. clinbiochem.2011.08.962.

[48] X. Zhao, P. Wu, M. Liu, D. Lu, J. Ming, C. Li, J. Ding, Q. Yan, and P. Fang, "Y_2O_3 modified TiO_2 nanosheets enhanced the photocatalytic removal of

4-chlorophenol and Cr (VI) in sun light," *Applied Surface Science*, vol. 410, pp. 134–144, 2017, doi: 10.1016/j.apsusc.2017.03.073.

[49] S. A. Salman, N. A. Bakr, and S. S. Abduallah, "Study of thermal decomposition and FTIR for PVA-AlCl composite films," *Journal of Engineering and Applied Sciences*, vol. 14, no. 3, pp. 717–724, 2019, doi: 10.36478/jeasci.2019.717.724.

[50] F. Houhoune, D. Nibou, S. Chegrouche, and S. Menacer, "Behaviour of modified hexadecyltrimethylammonium bromide bentonite toward uranium species," *Journal of Environmental Chemical Engineering*, vol. 4, no. 3, pp. 3459–3467, 2016, doi: 10.1016/j.jece.2016.07.018.

[51] Y. Xi, M. Mallavarapu, and R. Naidu, "Preparation, characterization of surfactants modified clay minerals and nitrate adsorption," *Applied Clay Science*, vol. 48, no. 1–2, pp. 92–96, 2010, doi: 10.1016/j.clay.2009.11.047.

[52] J. Zawadzki and H. Kaczmarek, "Thermal treatment of chitosan in various conditions, *Carbohydrate Polymers*, vol. 80, no. 2, pp. 394–400, 2010, doi: 10.1016/j.carbpol.2009.11.037.

[53] C. Peniche-Covas, W. Argüelles-Monal, and J. San Román, "A kinetic study of the thermal degradation of chitosan and a mercaptan derivative of chitosan," *Polymer Degradation and Stability*, vol. 39, no. 1, pp. 21–28, 1993, doi: 10.1016/0141-3910(93)90120-8.

[54] W. Payakgul, O. Mekasuwandumrong, V. Pavarajarn, and P. Praserthdam, "Effects of reaction medium on the synthesis of TiO_2 nanocrystals by thermal decomposition of titanium (IV) n-butoxide," *Ceramics International*, vol. 31, no. 3, pp. 391–397, 2005, doi: 10.1016/j.ceramint.2004.05.025.

[55] M. Gao, L. Zhu, W. L. Ong, J. Wang, and G. W. Ho, "Structural design of TiO_2-based photocatalyst for H_2 production and degradation applications," *Catalysis Science & Technology*, vol. 5, no. 10, pp. 4703–4726, 2015, doi: 10.1039/C5CY00879D.

[56] T. Lv, L. Pan, X. Liu, and Z. Sun, "Visible-light photocatalytic degradation of methyl orange by CdS-TiO_2–Au composites synthesized via microwave-assisted reaction," *Electrochimica Acta*, vol. 83, pp. 216–220, 2012, doi: 10.1016/j.electacta.2012.08.018.

[57] A. N. Ökte and Ö. Yılmaz, "Photodecolorization of methyl orange by yttrium incorporated TiO_2 supported ZSM-5", *Applied Catalysis B*, vol. 85, no. 1–2, pp. 92–102, 2018, doi: 10.1016/j.apcatb.2008.07.025.

[58] L. Alidokht, A. R. Khataee, A. Reyhanitabar, and S. Oustan, "Cr (VI) immobilization process in a Cr-spiked soil by zerovalent iron nanoparticles: Optimization using response surface methodology," *Clean: Soil, Air, Water*, vol. 39, no. 7, pp. 633–640, 2011, doi: 10.1002/clen.201000461.

[59] P. Chawla, S. K. Sharma, and A. P. Toor, "Optimization and modeling of UV-TiO_2 mediated photocatalytic degradation of golden yellow dye through response surface methodology," *Chemical Engineering Communication*, vol. 206, no. 9, pp. 1123–1138, 2019, doi: 10.1080/00986445.2018.1550392.

[60] H. Zangeneh, A. A. Zinatizadeh, S. Zinadinia, M. Feyzib, E. Rafieec, and D. W. Bahnemann, "A novel L-Histidine (C, N) codoped-TiO_2-CdS nanocomposite for efficient visible photo degradation of recalcitrant compounds from wastewater," *Journal of Hazardous Materials*, vol. 369, no. 384–397, 2019, doi: 10.1016/j.jhazmat.2019.02.049.